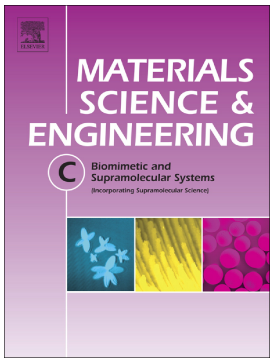

Fabrication of electrochemical biosensor consisted of multi-functional DNA structure/porous au nanoparticle for avian influenza virus (H5N1) in chicken serum

Taek Lee, Sun Yong Park, Hongje Jang, Ga Hyeon Kim, Yeonju Lee, Chulhwan Park, Mohsen Mohammadniaei, Min-Ho Lee, Junhong Min

PII: S0928-4931(18)33559-8
DOI: https://doi.org/10.1016/j.msec.2019.02.001
Reference: MSC 9394

To appear in: *Materials Science & Engineering C*

Received date: 22 November 2018
Revised date: 31 January 2019
Accepted date: 1 February 2019

Please cite this article as: T. Lee, S.Y. Park, H. Jang, et al., Fabrication of electrochemical biosensor consisted of multi-functional DNA structure/porous au nanoparticle for avian influenza virus (H5N1) in chicken serum, Materials Science & Engineering C, https://doi.org/10.1016/j.msec.2019.02.001

Fabrication of Electrochemical Biosensor Consisted of Multi-functional DNA Structure/porous Au Nanoparticle for Avian Influenza Virus (H5N1) in Chicken Serum

Taek Lee[a,*], Sun Yong Park[a], Hongje Jang[b], Ga Hyeon Kim[a], Yeonju Lee[a], Chulhwan Park[a], Mohsen Mohammadniaei[c], Min-Ho Lee[c,*], Junhong Min[c,*]

[a]*Department of Chemical Engineering, and* [b]*Department of Chemistry, Kwangwoon University, Wolgye-dong, Nowon-gu, Seoul 01899, Republic of Korea*

[c] *School of Integrative Engineering, Chung-Ang University, Heukseok-dong, Dongjak-gu, Seoul 06910, Republic of Korea*

*To whom co-correspondence should be addressed to

Prof. Taek Lee

Department of Chemical Engineering, Kwangwoon University

Tel.: (+82)2-940-5771; Fax: (+82)2-940-5771; E-mail address: tlee@kw.ac.kr

Prof. Min-Ho Lee

School of Integrative Engineering, Chung-Ang University

Tel.: (+82)2-820-5503; Fax: (+82)2-814-2651; E-mail address: mhlee7@cau.ac.kr

Prof. Junhong Min

School of Integrative Engineering, Chung-Ang University

Tel.: (+82)2-820-5348; Fax: (+82)2-814-2651; E-mail address: junmin@cau.ac.kr

Abstract

Avian influenza virus (AIV) is one of the most harmful pathogens to living things due to its fast infection, various mutations, and dangerous symptoms. In this study, we fabricated a label-free AIV H5N1 biosensor composed of multi-functional DNA structure on a porous Au nanoparticles (pAuNPs) fabricated electrode using the electrochemical (EC) technique. As a multi-functional bioprobe, the DNA 3 way-junction (3WJ) was introduced. Each fragment of DNA 3WJ was rolled to recognition part (hemagglutinin (HA) protein detection aptamer), EC signal generation part (horseradish peroxidase (HRP)-mimicked DNAzyme), and immobilization part (Thiol group). Each fragment was assembled in order to form the DNA 3WJ for AI detection and the assembled structure was confirmed by native-tris boric acid magnessim polyacrylamide gel electrophoresis (TBM-PAGE). Moreover, in order to increase the electrochemical signal sensitivity, pAuNPs were synthesized. The property of pAuNPs was investigated by field emission scanning electron microscopy (FE-SEM), Transmission electron microscopy (TEM), Ultraviolet–visible (UV-VIS) spectroscopy and zeta potential analysis. The DNA 3WJ on pAuNPs-modified Au electrode was then prepared using the layer-by-layer (LbL) assembly method. FE-SEM and atomic force microscopy (AFM) were used to investigate the surface morphology. Cyclic voltammetry (CV) was carried out to confirm the HA protein binding to DNA 3WJ-modified electrode. Moreover, The HA protein can be detected 1 pM in HEPES solution and 1 pM in diluted-chicken serum, respectively. The present study showed label-free, simple fabrication, and easy-to-tailor detection elements for AIV. The present biosensor can be a powerful candidate for various virus detection platforms.

Keyword: Avian influenza virus detection; Hemagglutinin; Multi-functional DNA structure; DNA 3 way-junction; Electrochemical biosensor; Porous Au nanoparticle

1. Introduction

As an acute infectious virus, the influenza virus has long threated humans and animals with a high fever, cough, chill, and other symptoms [1]. As the Fourth Industrial Revolution and world globalization have accelerated, the influenza virus has had a greater impact to public health in every country. Among them, the avian influenza virus (AIV) is one of the most serious viruses because of their acute infection, rapid spreading, respiratory illness, economic impact, and other reasons [2]. AIV can be classified to 4 types (A, B, C, D type). In particular, AIV (H5N1) virus can infect to a human from a bird [3]. In 1997, the first AIV infection of a human from a bird was reported in Hong Kong [4]. So far, H5N1 infection to the human was reported in 860 cases and 454 victims were reported. These symptoms are closely related with hemagglutinin (HA) protein [5]. The HA protein is the envelope protein of AIV that can bind to sialic acid receptors of cells. The HA protein is the one of the significant factors of viral infection from birds to humans. For this reason, the detection of HA protein is one of the important issues in AIV detection.

Several methods have been developed to identify H5N1. For example, the immunochromatography, the reverse-transcriptase polymerase chain reaction (RT-PCR) [7], enzyme-linked immunosorbent assay (ELISA) [8], serological methods [9], quartz crystal microbalance (QCM) [10], surface plasmon resonance (SPR) [11], and fluorescence [12] are typically laborious and time-consuming and are required to be conducted by specialized researchers. For constructing the portable field-ready H5N1 biosensor, the essential requirements meet the conditions of accuracy, high sensitivity, high throughput, specificity, rapid signal response time, small amount of target sample, and being easy to handle for on-site use. As a great alternative, the electrochemical (EC) detection method is suitable for meeting those criteria [13,14].

EC detection method can be easily combined with other technique such for photoelectrochemical biosensor [15,16]. Moreover, the EC technique gives a reliable response with a low cost, small sample volume without amplification step, and user-friendly interface and portability for detecting the H5N1 gene [17,18] and viral protein [19]. Several studies have reported the AIV detection using EC techniques.

The DNA aptamer is one of the most useful recognition probe for detecting AIV [20]. The DNA aptamer is cheap, simple, and small compared to antibody [10]. However, the aptamer-based AIV biosensor needs the additional labeling process and anchoring process that required complicated detection strategy. In order to solve this problem, the present study developed the EC-based biosensor composed of multi-functional DNA 3 way-junction (3WJ) structure and porous Au nanoparticles (pAuNPs) on Au electrode. The 3WJ motif-based DNA structure can be easily prepared and extended the functionality [21-23]. Compared to dsDNA, DNA 3WJ has an additional arm for embodying the extra functionality such as adding aptamer, redox reporter or thiol group, simultaneously [24,25].

Based on this structure, DNA 3WJ-a fragment was modified in order to introduce the HA protein aptamer (AIV detection part). Usually, the conventional EC-based biosensor used the enzyme such as horseradish peroxidase (HRP) for the electrochemical signal generation [26]. However, this enzyme-related virus detection required an additional conjugation step and an expensive labeling process. The HRP-mimicked DNAzyme with the hemin is a useful tool for simplifying the detection step [27]. It required the short oligonucleotide, cost-effective and similar redox property compared to enzyme. Shen et al reported electrochemical thrombin biosensor consisted of the G-quadruplex-based DNAzymes aptasensor with amplified electrochemical signal generation [28].

For this reason, the HRP-DNAzyme with hemin was incorporated into the DNA 3WJ fragment (DNA 3WJ-b) for the electrochemical signal generation function (redox reporter). The rest of the fragments of DNA 3WJ-c were introduced to thiol-groups for immobilizing the DNA 3WJ without additional linker material. The multi-functional DNA 3WJ can minimize the additional detection, amplification and labeling process compared to normal aptasensor. Moreover, to detect the low concentration of HA protein, pAuNPs were introduced to the electron transfer facilitation because of surface roughness enhancement and high adsorbability [29]. Synthesis of pAuNPs was demonstrated by field-emission scanning electron microscope (FE-SEM), transmission electron microscopy (TEM), ultraviolet-visible (UV-vis) spectroscopy, and hydrodynamic radius and ξ-potential. The immobilization process of multi-functional DNA 3WJ on pAuNPs-modified electrode was verified through atomic force microscopy (AFM). The electrochemical property and biosensor performance were investigated through cyclic voltammetry (CV). Fig. 1 showed a schematic diagram of the proposed biosensor.

2. Experimental details

2.1. Materials

The Influenza A H5N1 (A/VietNam/1203/2004) Hemagglutinin / HA Protein (His & Fc Tag) was purchased from Sino Biology (China). For pAuNPs immobilization, the chemical linkers, cysteamine, hemin, bovine serum albumin, troponin I and myoglobin were all purchased from Sigma-Aldrich (USA). The three fragments of DNA 3WJ were synthesized by Bioneer (South Korea). The sequence information of H5N1 HA aptamer -tagged 3WJ-a is 5'-GTG TGC ATG

GAT AGC ACG TAA CGG TGT AGT AGA TAC GTG CGG GTA GGA AGA AAG GGA AAT AGT TGT CCT GTT GTT GCC ATG TGT ATG TGG G -3', the HRPzyme-tagged 3WJ-b is 5'-TTTGGGTAGGGCGGGTTGGG CCCACATACTTTGTTGATCC -3', and Thiol-tagged 3WJ-c is SH-5'-GGATCAATCATGGCAA-3'. All oligonucleotides were diluted in the nuclease free water. The bare gold electrode (50 nm)/Cr (2 nm) on SiO_2 (5 mm) and biosensor electrode were fabricated by the National Nanofab Center (South Korea). The 4-(2-hydroxyethyl)-1-piperazineethanesulfonic acid (HEPES) was used as the buffer for electrochemical experimentation. Hydrogen tetrachloroaurate (III) hydrate was purchased from Kojima Chemicals Co. (Japan). Silver nitrate, hydrogen peroxide (30%), trisodium citrate dihydrate, and sodium borohydride were all purchased from Junsei (Japan). L-ascorbic acid, citric acid, and poly(vinylpyrrolidone) were all purchased from Sigma (USA). For clinical testing, the chicken serum was purchased from Thermo Fisher Scientific (USA). All chemicals were used as received.

2.2. Synthesis of pAuNPs

Preparation of Ag nanoseed, 250 μL of 10 mM $AgNO_3$, 300 μL of 30 mM trisodium citrate dihydrate, 1.5 mL of 3.5 mM poly(vinylpyrrolidone) (PVP, MW: 29 kDa), and 24.75 mL of DI water were added to a 50 mL glass vial. Next, 60 μL of 30% hydrogen peroxide was added and magnetically stirred for 3 min at ambient condition. The Ag nanoseed growth was accomplished by the rapid addition of 250 μL of 100 mM sodium borohydride aqueous solution. Along with 3 hr of incubation at room temperature, the solution color was gradually changed from transparent, light yellow to blue. After the depletion of added $NaBH_4$, it proceeded to the Ag nanoseed growth step without any treatment or purification [30]. Then, the growth of template Ag nanoplates

process was conducted. In order to prepare Ag nanoseeds solution, 0.333 mL of 75 mM sodium citrate and 1 mL of 100 mM L-ascorbic acid aqueous solutions were added under magnetic stirring. Meanwhile, a growth solution composed of 20 mL of 1 mM $AgNO_3$, 0.125 mL of 100 mM citric acid, and 10 μL of 75 mM sodium citrate was prepared in another vial. To the Ag nanoseeds solution, 13 mL of as-prepared growth solution was added by 0.1 mL/sec of injection time. Along with the addition, solution color was gradually changed into deep-blue. After 10 min of further incubation, synthesized Ag nanoplates were used as template for galvanic replacement without further purification process. As-synthesized Ag nanoplates solution was five-fold diluted by DI water, then 20 v/v% of 1 mM $AuCl_4^-$ aqueous solution was rapidly injected and vigorously inverted several times to ensure homogeneous mixing. Solution color was changed in the course of pale blue, purple, and deep-blue within 30 min from replacing ion addition. After 2 hr of sufficient incubation at ambient condition, product was purified by centrifugation at 9000 rpm for 10 min and washed with DI water more than three times.

pAuNP is manufactured by reducing agent assisted excessive galvanic replacement of sacrificial Ag nanoplate templates. Conventional galvanic replacement is accomplished by a spontaneous redox reaction between an oxidation-favored Ag nanotemplate and a reduction-favored metal cation. However, addition of excessive replacing ions generally caused structural collapse or aggregation due to uncontrollable dissolution of template. In the preparation of pAuNP, the reducing additive (L-ascorbic acid) and surface stabilization substances (citrate and polyvinylpyrrolidone) present in the reaction solution induced secondary surface growth based on the as-synthesized Au nanoskeletals from the very first galvanic replacement reaction. Due to the competitive role of replacement and reductive secondary growth, a porous nanoplatelet structure

is formed without colloidal destabilization. Finally, pAuNPs were re-dispersed into 40 mL of DI water and denoted the concentration as 1 eq.

2.3 Characterization of pAuNPs

Energy-filtering transmission electron microscope LIBRA 120 (Carl Zeiss, Germany), field-emission scanning electron microscope AURIGA (Carl Zeiss, Germany), and Tecnai F20 S/TEM (FEI, Hillsboro, OR, USA) were used to obtain electron microscope images. UV-Vis spectrophotometer Lambda 465 (PerkinElmer, USA) was used to obtain UV-Vis-NIR extinction spectrum. Hydrodynamic radius and ζ-potential were measured by Zetasizer Nano ZS (Malvern, UK).

2.4. Assembly of multi-functional DNA 3WJ nanostructure

The proposed biosensor was composed of multi-functional DNA structure to simplify the detection step. For the HA protein detection part, the H5N1 AI aptamer-tagged DNA 3WJa (AI Apt/3WJa, 5’-GTG TGC ATG GAT AGC ACG TAA CGG TGT AGT AGA TAC GTG CGG GTA GGA AGA AAG GGA AAT AGT TGT CCT GTT GTT GC CAT GTG TA TGT GGG -3’) was introduced. The aptamer sequence was followed by Shiratory’s work [20]. For the electrochemical signal generation part, the G-quadruplex HRP-mimicking DNAzyme with hemin-tagged DNA 3WJb was introduced (Zyme/3WJb, 5'- TTT GGG TAG GGC GGG TTG GGC CCA CAT ACT TTG TTG ATC C -3'). For, the immobilization part, thiol-modified DNA 3WJc was prepared (SH/3WJc, SH-5'-GGA TCA ATC ATG GCA A-3’). Those sequences were chemically

synthesized from Bioneer (South Korea). The AIapt/Zyme/SH-3WJ was assembled by annealing three corresponding DNA strands at equal molar ratio in TMS buffer (50 mM Tris-HCl, 10 mM $MgCl_2$, 100 mM NaCl) by heating at 80ºC for 5 min, followed by slowly cooling down to 4ºC at a rate of 2ºC/min on a T100™ Thermal Cycler (Bio-rad). The multi-functional DNA 3WJ assembly was confirmed by 8% native polyacrylamide gel prepared in TBM buffer (89 mM Tris, 200 mM boric acid, 2 mM $MgCl_2$, pH 7.6). About 0.2 μg of DNA samples were loaded into each lane. After running at 100 V for 90 mins, the DNA assembly were visualized by ethidium bromide staining [23].

2.5. Electrode Fabrication

The P-type 4-inch Si substrate (100) with a thermally oxidized SiO_2 was initially cleaned using a piranha solution composed of H_2SO_4 (Daejung Chemical and Metals Co. Ltd., South Korea) and H_2O_2 (Daejung Chemical and Metals Co. Ltd., South Korea) with a volume ratio of 7:3 for 5 min at room temperature and baked on the hot plate at 200°C for 20 min for adhesion promotion with photoresist. The metal deposition of pre-pattern was prepared by the standard photolithographic process using negative photoresist. Su-82 photoresist was spin-coated onto the substrate with a 3000 rpm, then baked at 65°C for 1 min and 95°C for 1 min. After exposure of 110 mJ/cm^2 (i-line) by MA6 mask aligner (SUSS MicroTec, Germany), substrate was post-baked by the same steps with pre-baking and developed for 70s. Metal deposition of Cr (2 nm) and Au (50 nm) was carried out with an electron beam evaporator. Finally, a lift-off process was performed using remover PG at 70°C for 2 hr. The fabricated biosensor electrode was cleaned with piranha solution under the

same conditions. For the electrochemical analysis, the working chamber was prepared by PDMS linkage and attached to the electrode. After attachment of the chamber on the electrode, substrates were washed by ethanol and DI water to remove organic contaminant, which could be induced in the curing process of PDMS at high-temperature chamber [31]. Fig. 2 (a) – (d) shows a schematic diagram, CAD image, and optical image of the fabricated electrode as well as a real picture of the fabricated AIV biosensor.

2.6. Fabrication and investigation of multi-functional 3WJ/pAuNPs heterolayer

In order to fabricate a DNA 3WJ/pAuNPs heterolayer, the prepared Au electrode was treated with acetone solution with sonication for 5 min, washed with ethanol and deionized water, and dried under N_2 gas to remove residues before the self-assembly process [32]. The 3 μl of 5% cysteamine was added to substrate. And, The 3 μl of 5 eq pAuNP was dropped onto modified substrate. Then, 3 μl of 1 uM 3WJ with 3 μl of 1 mM of hemin solution was added onto the Au surface for 12 hr. The thiol group of the 3WJ molecule was anchored to the Au surface by covalent bonding during the immobilization process. Hemin has the iron-containing porphyrin with chlorine that can be enabled to redox signal generation. During this step, the free hemin molecule was formed between Fe ion in hemin and π–π stacking in G-quadruplex DNA to catalyze the electrochemical activity [28]. The modified substrates were cleaned with deionized water and dried under an N_2 gas stream.

2.7 Surface morphology analysis

The surface of multi-functional DNA 3WJ on pAuNPs electrode was investigated by AFM using Nanoscope IV / Multimode (Digital Instruments, USA). The bare Au substrate, pAuNPs-immobilized substrate, and pAuNPs-modified substrate were characterized for comparison. Phosphorous (n-type doped Si, RTESP, Bruker, USA) tips were used for the AFM measurement, and the resonance peaks in the frequency response of the cantilever were selected at around of 230-305 kHz. Spring constants of 20–80 N/m were used. Before scanning the sample, the set point current, integrated gain and proportional gain were optimized to the force between the tip and the biomolecule. By scanning electron microscopy (SEM) (Auriga, Carl Zeiss, Germany), surface morphology of pAuNPs immobilized electrode was also investigated [30].

2.8. Biosensor analysis of multi-functional DNA 3WJ/pAuNPs heterolayer

Cyclic voltammetry (CV) experiment was performed with a three-electrode system. The DNA 3WJ/pAuNPs/Au electrode was used as the working electrode, a Pt wire and an Ag/AgCl electrode were used as the counter and reference electrode, respectively. All Experiments were performed using a Versastat 3 potentiostat (Princeton Applied Research, USA).

3. Results and Discussion

3.1. Investigation of pAuNPs

First, we synthesized porous Au nanoplates (pAuNPs) using the previously reported reducing agent-assisted excessive galvanic replacement method [30]. In brief, after preparing the Ag nanoplates to be used as a template by seed-growth procedure, galvanic replacement reaction was

carried out by adding $AuCl_4^-$ ion without further treatment or purification. In this process, nanostructure framework was formed by the rapid initial replacement reaction, then, secondary growth was accomplished to formation of porous nanostructures by the existing reducing agents. Manufactured pAuNPs were characterized by transmission electron microscopy (TEM) and UV-Vis spectrophotometer in order to verify their morphology and optical properties. According to the TEM images, manufactured pAuNPs exhibited 60-110 nm diameter distribution (n = 100). (Fig. 3 (a)) High-resolution (HR) TEM observation clearly showed the rough and porous morphology of pAuNPs with polycrystallinity from galvanic replacement reaction. UV-Vis spectrum represented distinctive localized surface plasmon resonance (LSPR) from 500 nm to near-infrared region which implied clustering and networking mediated extinction bathochromic shift against conventional Au nanospheres. (Fig. 3 (b)) We also performed dynamic light scattering (DLS) measurement to determine the hydrodynamic radius of pAuNPs in DI water. Due to the Stokes-Einstein equation, which assumes the morphology of the particle as a spherical shape, the overall diameter distribution was lower than that of the nanoplate structures observed by electron microscope. However, it could be concluded that it is relatively homogeneously synthesized through the overall diameter distribution tendency. (Fig. 3 (c), left) A series of measurements additionally exhibited the ζ-potential (-20.2 ± 0.3 mV), polydispersity index (PDI: 0.162 ± 0.005), and electrophoretic mobility (-1.492 ± 0.031 μm cm V^{-1} s^{-1}) of pAuNPs. (Fig. 3 (c), right). Also, to confirm the uniformity and washing effect of pAuNP-immobilization onto Au substrate, FE-SEM analysis was carried out (Fig. S1, Fig. S2), respectively.

3.2. Construction of multi-functional DNA 3WJ

For contructing multi-functional bioprobe for detection HA protein, the aptamer was integrated into DNA 3WJa motif. The AI aptamer-target HA protein reactivity and the DNA 3WJ assembly were confirmed by 8% native TBM-PAGE with EtBr staining and coomassie staining, respectively (Fig. S3, Fig. S4). And the HRPzyme was combined to DNA 3WJb motif for EC signal generating with hemin. Finally, The thiol-modified DNA 3WJc was prepared for immobilization process without additional linker. Fig. 4 (a) described the expected AIapt/Zyme/SH-DNA 3WJ 2D structure. The assembly of AIapt/Zyme/SH-DNA 3WJ was confirmed by 8% native TBM-PAGE. Fig. 4 (b) shows the PAGE gel of the AIapt/Zyme/SH-DNA 3WJ assembly. The gel shows the AIapt-3Wja (lane 2), HRPzyme-3WJb (lane 3), SH-3WJc (lane 4) and AIapt/Zyme/SH-DNA 3WJ (lane 5) well. This result shows the designed multi-functional bioprobe can be easily integrated. Moreover, the designed bioprobe should retain the target recognition. In order to test this effect, the target HA protein was reacted with assembled AIapt/Zyme/SH-DNA 3WJ. Lane 7 shows the migration change and upper band occured that gives the assembled AIapt/Zyme/SH-DNA 3WJ bound the HA protein. In addition, as the negative control, the myoglobin was reacted with assembled AIapt/Zyme/SH-DNA 3WJ (lane 9). In this case, there was no migration change compared to lane 5. That means the assembled AIapt/Zyme/SH-DNA 3WJ did not bound with myoglobin. Then, the enzyme-linked immunosorbent assay (ELISA) was carried out so as to confirm the activity of AIapt/Zyme/SH-DNA 3WJ with hemin (Fig. S5). Based on the combined results, the designed bioprobe can detect the HA protein specifically.

3.3. Investigation of fabricated HA protein/multi-functional DNA 3WJ on pAuNPs heterolayer

The immobilization process of HA protein/multi-functional DNA 3WJ on pAuNPs heterolayer on the Au electrode was investigated by AFM and FE-SEM. Fig. 5 (a) displayed AFM results of pAuNPs-immobilized Au electrode. Because of the high surface roughness of pAuNP, Even though, AFM image showed the low resolution compared to TEM image (Fig. 3a). But, AFM analysis can provide the horizontal size, vertical size and surface roughness information of immobilized nanoparticles and biomolecules. In case of the horizontal size of pAuNPs, the sizes are observed around 60 - 100 nm. In case of vertical size analysis of pAuNPs, it is hard to determine the single nanoparticle analysis because of surrounding pAuNPs that hamper the analysis. Fig. S6 displayed the vertical size analysis of single pAuNP indicated the vertical distance between top of pAuNP and substrate is around 79.464 nm. The AFM result of the pAuNPs-modified electrode exhibited the porous nanoparticle morphology well. In addition, the additional FE-SEM images and AFM images of pAuNP-modified Au substrate with large area in supplementary materials (Fig. S1, Fig. S7). Fig. 5 (b) showed the multi-functional DNA 3WJ immobilized on pAuNPs/Au electrode. It formed small lumps with sizes around 20-30 nm, so it can be assumed the multi-functional DNA 3WJ was immobilized on the pAuNPs. In case of vertical analysis, the vertical sizes of multi-functional DNA 3WJ are around 6.514 ± 1.711 nm (Fig. S8 (a)). When the HA protein was immobilized, the AFM morphology was totally changed with large biomolecule aggregates (70-80 nm size) compared to DNA 3WJ molecule using horizontal analysis. In case of vertical analysis, the vertical size of HA protein we measured is around 10.630 ± 2.663 nm (Fig. S8 (b)). Fig. 5 (d) displayed the SEM image of fabricated pAuNPs/Au electrode. Also, the surface roughness and vertical distance analysis were carried out (Fig. 5 (e)). Based on the results, the prepared heterolayer was well prepared.

3.4. Electrochemical properties

Cyclic voltammetry (CV) was carried out to compare the feasibility test of enhanced redox properties of the AIapt/Zyme/SH-DNA 3WJ and AIapt/Zyme/SH-DNA 3WJ with with the HA protein immobilized on Au substrate (0.7 x 2 cm). As shown in Fig. 6 (a), the redox property of the AIapt/Zyme/SH-DNA 3WJ with hemin showed a quasi-reversible redox peaks (Green line) because of the $Fe^{3+/2+}$ redox center of hemin facilitated the electron transfer. The anodic peak point of potential (Epa) and anodic peak point of current (Ipa) values were showed at 484 mV and 2.68 μA (vs. Ag/AgCl), respectively. In addition, the cathodic peak point of potential (Epc) and cathodic peak point of current (Ipc) values were showed at 261 mV and -0.54 μA (vs. Ag/AgCl), respectively. The peak-to-peak separation (ΔEp) was 223 mV. When the HA protein was added to the AIapt/Zyme/SH-DNA 3WJ electrode (Blue line), the redox current values were decreased slightly. The anodic peak point of potential (Epa) and anodic peak point of current (Ipa) values were shown at 468 mV and 2.68 μA (vs. Ag/AgCl), respectively. In addition, the cathodic peak point of potential (Epc) and cathodic peak point of current (Ipc) values were showed at 265 mV and -0.54 μA (vs. Ag/AgCl), respectively. The red line shows the results of bare Au electrode. However, when the pAuNPs were introduced, the redox current discrepancy was significantly increased. Fig. 6 (b) shows the cyclic voltammogram of AIapt/Zyme/SH-DNA 3WJ (Green line) and AIapt/Zyme/SH-DNA 3WJ with the HA protein (Blue line) immobilized on pAuNPs-modified Au electrode, pAuNPs-modified electrode (Orange line) and bare Au electrode (Red line), respectively. In the case of AIapt/Zyme/SH-DNA 3WJ on pAuNPs, the anodic peak point of

potential (Epa) and anodic peak point of current (Ipa) values were shown at 325 mV and 1.17 μA (vs. Ag/AgCl), respectively. In addition, the cathodic peak point of potential (Epc) value and cathodic peak point of current value (Ipc) were shown at 112 mV and -1.06 μA (vs. Ag/AgCl), respectively. However, the AIapt/Zyme/SH-DNA 3WJ on pAuNPs with the HA protein displayed the decreased redox currents clearly compared to without target. The anodic peak point of potential (Epa) and point of current values were observed at 302 mV and 0.86 μA (vs. Ag/AgCl), respectively. In addition, the cathodic peak potential (Epc) and cathodic peak current (Ipc) values were showed at 110 mV and -0.79 μA (vs. Ag/AgCl), respectively. Based on the combined results, the pAuNPs-modified electrode can strongly facilitate the electron transfer that provides the signal-enhanced electrochemical AI detection biosensor platform. This result showed that the pAuNPs provides the higher surface roughness and active area which yielded a higher coverage [33-35].

Additionally, the CVs of the AIapt/Zyme/SH-DNA 3WJ on pAuNPs-modified electrode were observed with different scan rates from 10 to 70 mV/s (Fig. 6 (c)). The CV results showed well-defined and shifted cathodic and anodic peaks slightly at each scan rate. And, the CV result shows a linear plot for anodic and cathodic peak currents against the scan rate (Fig. 6 (d)), respectively. The linear regression equations of results were i_{pa} *(μA) = 2E-05 υ (mV/s) + 4E-08* for anodic currents and i_{pc} *(μA) = ipc (μA) = -1E-05 υ (mV/s) – 8E-08* for cathodic currents. The linearity of the graphs related to the scan rate (υ) showed the scan rate increment yields a slight shift of the cathodic peak to a more negative potential, while the anodic peak was moved to a more positive potential.

The charge transfer coefficient (α) value was found to be 0.529 based on the straight fitting lines extracted from the plotting of the anodic- and cathodic-potential peaks as a function of the log (υ) based on the regression equations of: *Epa = 0.033 log υ + 0.397 and Epc = 0.0293 log υ + 0.114, respectively.* Considering that, k_c = - *2.3 RT/αnF* and k_a = *2.3 RT/(1-α)nF,* in which k_c (0.0293) corresponds to the slope of $E_{pc} = f(\log \upsilon)$ and k_a (0.033), attributed to the slope that is deduced from $E_{pa} = f(\log \upsilon)$, the "$\alpha$" was calculated using the following equation [36]:

$$\log \frac{k_a}{k_c} = \log\left[\frac{\alpha}{(1-\alpha)}\right] or \frac{k_a}{k_c} = \frac{\alpha}{1-\alpha} \quad (1)$$

Moreover, the apparent electron-transfer-rate constant (k_s) between the pAuNPs-modified electrode and the surface AIapt/Zyme/SH-DNA 3WJ was determined as 0.42 s^{-1}, according to the following equation: (1)

$$\log k_s = \alpha \log(1-\alpha) + (1-\alpha)\log\alpha - \log\left(\frac{RT}{nF\nu}\right) - \frac{\alpha(1-\alpha)nF\Delta E_p}{2.3RT} \quad (2)$$

Where F is the Faraday constant, R is the gas constant, n is the number of electrons, and ΔE_p is the peak-to-peak separation of the redox potentials peaks ($\Delta E_p \approx 159$ mV).

In addition, the surface concentration (Γ) of DNA molecules on the fabricated substrate could be estimated as 7.3×10^{-11} mol/cm^{-2} based on the following equation [37]:

$$\Gamma = Q/nFA \quad (3)$$

Where Γ is the surface coverage of the DNA on the electrode, Q is the consumed charge (area under the reduction peak), v is the scan rate (0.05 $V.s^{-1}$), n is the number of electrons (n=1), F is the Faraday constant (96,500 $C.mol^{-1}.e^{-1}$). And A is the area of the electrode (0.25 cm^2). In addition,

the catalytic property of fabricated AIapt/Zyme/SH-DNA 3WJ with hemin was investigated with H_2O_2 addition by CV and DPV (Fig. S9). Also, to confirm the electrochemical decrement effect when the HA protein reacted to multi-functional DNA 3WJ with aptamer, the additional CV experiment was carried out (Fig. S10).

3.5. Biosensor performance and Clinical Test

CV experiments were carried out in order to evaluate the LOD and dynamic range of the proposed sensor in HEPES solution and chicken serum. In order to analyze LOD of biosensor, the bioprobe-modified electrode was reacted to the HA protein for 2 hr at RT. After the washing step, the electrodes were measured. As shown in Fig. 7 (a) (Yellow line) and 7 (b) (Yellow line), the EC signal of the HA protein concentration (1 pM to 100 nM). The redox peaks of AIapt/Zyme/SH-DNA 3WJ increased with decreasing target HA protein concentration. This phenomenon indicated relevance of HA protein binding to the AIapt/Zyme/SH-DNA 3WJ that hamper the electron transfer due to presence of HA protein on the bioprobe-modified electrode. The LOD of fabricated biosensor was observed to 9.43 pM in HEPES buffer. The regression equations were Δipa (μA) = -2E-08 lnC (pM) + 3E-07, R^2 = 0.8895 and Δipc (μA) = 2E-08 lnC (pM) - 4E-07, R^2 = 0.9062, respectively. In the case of clinical test, LOD test was carried out in the diluted chicken serum (Fig. 7 (a) (Green line), 7 (b) (Green line)). The regression equations were Δipa (μA) = -2E-08 lnC (pM) + 4E-07, R^2 = 0.9659 and Δipc (μA) = 2E-08 lnC (pM) - 4E-07, R^2 = 0.9869, respectively. The fabricated biosensor can detect the 1 pM of HA protein in HEPES buffer and 1 pM of HA protein diluted-chicken serum, respectively. The relative standard deviation (RSD) was

determined from 1.36 to 6.23 % that demonstrated a highly reproducibility of proposed biosensor. Moreover, the specificity of the proposed biosensor investigated by introducing other proteins such as BSA, troponin I and myoglobin as the negative control experiments. There is little EC signal change observed in other protein test (Fig. 7 (c), (d)). Moreover, the durability and test was carried out (Fig. S11). The result can be elucidated the proposed AIapt/Zyme/SH-DNA 3WJ have the specificity to HA protein well. A comparison between present AIV biosensor and other biosensors reported is summarized in Table 1 [38,39]. To our best knowledge, Hushegyi et al reported the glycan-based AIV H3N2 detection with 5 aM of LOD [32]. The proposed detection system comprised with DNA 3WJ/pAuNPs didn't show the lowest LOD. However, the proposed work might reduce the redox reporter labeling step and signal amplification step. Even, the dsDNA can be tagged to the AI aptamer and thiol group without redox agent, however, we still believe the advantage of DNA 3WJ has the extending their functionalities such as multiple-target detection biosensor in one platform or one target detection using dual detection method with high reliability [40,41]. For example, DNA 3WJ/pAuNP platform could be applied to the dual aptamer-tagged bioprobe with linker to determine the sub-type of AI virus (H5N1, H1N1) in one platform or H5N1 biosensor using electrochemical and colorimetric dual-detection method.

4. Conclusions

The present study developed the EC-based label-free AIV detection method using multi-functional DNA structure on pAuNPs-modified electrode. Each fragment of DNA embodied to the specific functionality such as HA protein detection, EC signal generation, and immobilization.

Those nucleic acid fragments assembled well without loss of functionality. That confirmed by several electrophoresis experiments. And pAuNPs were easily synthesized and confirmed by TEM, FE-SEM and other tests. This nanomaterial was introduced to Au electrode for the EC signal facilitation materials effectively. AFM and FE-SEM used to investigate the surface topography. The CV was conducted to confirm the HA protein binding to DNA 3WJ/pAuNPs-modified electrode. Moreover, HA proteins were detected by fabricated biosensor in the HEPES buffer and chicken serums, respectively. Although, some EC-based AIV detection methods were proposed, however, the present work did not require additional labeling process and signal amplification process compared to previous works. The present study provided a label-free, redox reporter free, simple fabrication and easy-to-tailored detection bioprobe for AI virus. Thus, the proposed DNA 3WJ/pAuNPs-based detection method could be applied for the multiple-target detection biosensor for determining the pathogen subtype in one platform or one target detection using dual detection method with high reliability.

Acknowledgments

*This research was supported by Basic Science Research Program through the National Research Foundation of Korea (NRF) funded by the Ministry of Education (2018R1D1A1B07049407) and by the BioNano Health-Guard Research Center funded by the Ministry of Science and ICT (MSIT) of Korea as a Global Frontier Project (Grant number H-GUARD_2018M3A6B2057261) and by the Republic of Korea (Goverment-wide R&D Fund project for infectious disease research, HG18C0012).

References

1. B. Panigrahy, D. A. Senne, J. C. Pedersen, A. L. Shafer, J. E. Pearson, Susceptibility of pigeons to avian influenza. Avian Dis. 40 (1996) 600-604.

2. J. K. Thomas, J. Noppenberger, Avian influenza: a review. Am. J. Health Syst. Pharm. 64 (2007) 149-165.

3. D. L.Suarez, S. Schultz-Cherry, Immunology of avian influenza virus: a review. Dev. Comp. Immunol. 24 (2000) 269-283.

4. T. M. Uyeki, Human infection with highly pathogenic avian influenza A (H5N1) virus: review of clinical issues. Clin. Infect. Dis. 49 (2009) 279-290.

5. H. Yang, P. J. Carney, V. P. Mishin, Z. Guo, J. C. Chang, Wentworth, D. E.; Gubareva, L. V.; Stevens, J. The molecular characterizations of surface proteins hemagglutinin and neuraminidase from recent H5Nx avian influenza viruses. J. Virol. 90 (2016) 5770-5784.

6. Y. Tsuda, Y. Sakoda, S. Sakabe, T. Mochizuki, Y. Namba, H. Kida, Development of an immunochromatographic kit for rapid diagnosis of H5 avian influenza virus infection. Microbiol. Immunol. 51 (2007) 903-907.

7. E. Spackman, D. A. Senne, L. L. Bulaga, T. J. Myers, M. L. Perdue, L. P. Garber, K. Lohman, L. T. Daum, D. L. Suarez, Development of real-time RT-PCR for the detection of avian influenza virus. Avian Dis. 47 (2003) 1079-82.

8. D. S. Song, Y. J. Lee, O. M. Jeong, Y. J. Kim, C. H. Park, J. E. Yoo, W. J. Jeon, J. H. Kwon, G. W. Ha, B. K. Kang, C. S. Lee, H. K. Kim, B. Y. Jung, J. H. Kim, , J. S. Oh, Evaluation of a

competitive ELISA for antibody detection against avian influenza virus. J. Vet. Sci. 10 (2009) 323-329.

9. A. Comin, N. Toft, A. Stegeman, D. Klinkenberg, S. Marangon, Serological diagnosis of avian influenza in poultry: is the haemagglutination inhibition test really the 'gold standard'?. Influenza Other Respir. Viruses. 7 (2013) 257-264.

10. L. Xu, R. Wang, L. C. Kelso, Y. Ying, Y. Li, A target-responsive and size-dependent hydrogel aptasensor embedded with QD fluorescent reporters for rapid detection of avian influenza virus H5N1, Sens. Actuators B. 234 (2016) 98-108.

11. H. Bai, R. Wang, B. Hargis, H. Lu, Y. Li, A SPR Aptasensor for detection of avian influenza virus H5N1, Sensors 12 (201) 12506-12518.

12. Y. Pang, Z. Rong, J. Wang, R. Xiao, S. Wang, A fluorescent aptasensor for H5N1 influenza virus detection based-on the core-shell nanoparticles metal-enhanced fluorescence (MEF), Biosens Bioelectron. 66 (2015) 527-532.

13. I. Grabowska, K. Malecka, U. Jarocka, J. Radecki, H. Radecka, Electrochemical biosensors for detection of avian influenza virus-current status and future trend, Acta. Biochim. Pol. 61 (2014) 471-478.

14. Y. Tepeli, A. Ülkü, Electrochemical biosensors for influenza virus a detection: The potential of adaptation of these devices to POC systems, Sens. Actuators B. 254 (2018) 377-384.

15. M. Li, C. Xiong, Y. Zheng, W. Liang, R. Yuan, Y. Chai, Ultrasensitive photoelectrochemical biosensor based on DNA tetrahedron as nanocarrier for efficient immobilization of CdTe QDs-methylene blue as signal probe with near-zero background noise, Anal. Chem., 90 (2018) 8211-

8216.

16. Z. Luo, L. Zhang, R. Zeng, L. Su, D. Tang, Near-infrared light-excited core–core–shell UCNP@Au@CdS upconversion nanospheres for ultrasensitive photoelectrochemical enzyme ummunoassay, Anal. Chem., 90 (2018) 9568-9575.

17. X. Liu, Z. Cheng, H. Fan, S. Ai, R. Han, Electrochemical detection of avian influenza virus H5N1 gene sequence using a DNA aptamer immobilized onto a hybrid nanomaterial-modified electrode, Electrochim. Acta. 56 (2011) 6266- 6270.

18. X. Zhu, S. Ai, Q. Chen, H. Yin, J. Xu, Label-free electrochemical detection of avian influenza virus genotype utilizing multi-walled carbon nanotubes–cobalt phthalocyanine–PAMAM nanocomposite modified glassy carbon electrode, Electrochem. Commun. 11 (2009) 1543-1546.

19. M. Veerapandian, R. Hunter, S. Neethirajan, Dual immunosensor based on methylene blue-electroadsorbed graphene oxide for rapid detection of the influenza A virus antigen, Talanta. 155 (2016) 250–257.

20. I. Shiratori, J. Akitomi, D. A. Boltz, K. Horii, M. Furuichi, I. Waga, Selection of DNA aptamers that bind to influenza A viruses with high affinity and broad subtype specificity, Biochem. Biophys. Res. Commun. 443 (2014) 37-41.s

21. F. Li, Y. Lin, X. C. Le, Binding-Induced Formation of DNA Three-Way Junctions and Its Application to Protein Detection and DNA Strand Displacement, Anal. Chem. 85 (2013) 10835-10841.

22. Y. Xia, S. Gan, Q. Xu, X. Qiu, P. Gao, S. Huang, A three-way junction aptasensor for lysozyme

detection, Biosens. Bioelectron. 39 (2013) 250-254.

23. T. Lee, A. K. Yagati, F. Pi, A. Sharma, J. W. Choi, P. Guo, Construction of RNA–quantum dot chimera for nanoscale resistive biomemory application, ACS Nano. 9 (2015) 6675-6682.

24. B. Liu, J. Chen, Q. Wei, B. Zhang, L. Zhang, D. Tang, Target-regulated proximity hybridization with three-way DNA junction for in situ enhanced electronic detection of marine biotoxin based on isothermal cycling signal amplification strategy, Biosens. Bioelectron. 15 (2015) 241-248.

25. B. Liu, B. Zhang, G. Chen, H. Yang, D. Tang, Proximity ligation assay with three-way junction-induced rolling circle amplification for ultrasensitive electronic monitoring of concanavalin A, Anal. Chem. 86 (2014) 7773-7781.

26. S. Campuzano, P. Yáñez-Sedeño, J. M. Pingarrón, Molecular Biosensors for Electrochemical Detection of Infectious Pathogens in Liquid Biopsies: Current Trends and Challenges, Sensors. 17 (2017) 2533.

27. G. Pelossof, R. Tel-Vered, J. Elbaz, I. Willner, Amplified biosensing using the horseradish peroxidase-mimicking DNAzyme as an electrocatalyst, Anal. Chem. 82 (2010) 4396-4402.

28. B. Shen, Q. Wang, D. Zhu, J. Luo, G. Cheng, P. He, Y. Fang, G-quadruplex-based DNAzymes aptasensor for the amplified electrochemical detection of thrombin, Electroanalysis 22 (201) 2985 -2990.

29. O. V. Shulga, K. Jefferson, A. R. Khan, V. T. D'Souza, J. Liu, A. V. Demchenko, K. J. Stine, Preparation and characterization of porous gold and its application as a platform for immobilization of acetylcholine esterase, Chem Mater. 19 (2007) 3902-3911.

30. S. Kang, K. Kang, H. Huh, H. Kim, S. J. Chang, T. J. Park, K. S. Chang, D. H. Min, H. Jang, Reducing Agent-Assisted Excessive Galvanic Replacement Mediated Seed-Mediated Synthesis of Porous Gold Nanoplates and Highly Efficient Gene-Thermo Cancer Therapy, ACS Appl. Mater. Interfaces. 9 (2017) 35268-35278.

31. T. Lee, Y. Lee, S. Y. Park, K. Hong, Y. Kim, C. Park, Y. -H. Chung, M. -H. Lee, J. Min, Fabrication of electrochemical biosensor composed of multi-functional DNA structure/Au nanospike on micro-gap/PCB system for detecting troponin I in human serum, Colloids Surf. B. 175 (2019) 343 -350.

32. T. Lee, S. U. Kim, J. Min, J. W. Choi, Multilevel biomemory device consisting of recombinant azurin/cytochrome c, Adv. Mater. 22 (2010) 510-514.

33. J. M. Pingarron, P. Yanez-Sedeno, A. Gonzalez-Cortes, Gold nanoparticle-based electrochemical biosensors, Electrochimica Acta. 53 (2008) 5848-5866.

34. S. Karash, R. Wang, L. Kelso, H. Lu, T. J. Huang, Y. J. Li, Rapid detection of avian influenza virus H5N1 in chicken tracheal samples using an impedance aptasensor with gold nanoparticles for signal amplification, Virol. Methods. 236 (2016) 147-156.

35. R. Zhang, H. Olin, Porous Gold Films-A Short Review on Recent Progress, Materials 7 (2014) 3834-3854.

36. E. Laviron, General expression of the linear potential sweep voltammogram in the case of diffusionless electrochemical systems, J. Electroanal. Chem. Interfacial Electrochem, 101 (1979) 19-28.

37. H. Razmi, M. Harasi, Voltammetric behavior and amperometric determination of ascorbic acid

at cadmium pentacyanonitrosylferrate film modified GC electrode, Int. J. Electrochem. Sci. 3 (2008) 82-95.

38. A. Hushegyi, D. Pihikova, T. Bertok, V. Adam, R. Kizek, J. Tkac, Ultrasensitive detection of influenza viruses with a glycan-based impedimetric biosensor, Biosens. Bioelectron. 79 (2016) 644-649.

39. U. Jarocka, R. Sawicka, A. Gora-Sochacka, A. Sirko, W. Dehaen, J. Radecki, H. Radecka, An electrochemical immunosensor based on a 4, 4'-thiobisbenzenethiol self-assembled monolayer for the detection of hemagglutinin from avian influenza virus H5N1, Sens. Actuators B. 238 (2016) 25-30.

40. B. Ng, E. J. H. Wee, N. P. West, M. Trau, Naked-eye colorimetric and electrochemical detection of Mycobacterium tuberculosis − towards rapid screening for active case finding, ACS Sens., 1 (2016) 173-178.

41. N. Paniel, J. Baudart, Colorimetric and electrochemical genosensors for the detection of Escherichia coli DNA without amplification in seawater, Talanta 115 (2013) 133-142.

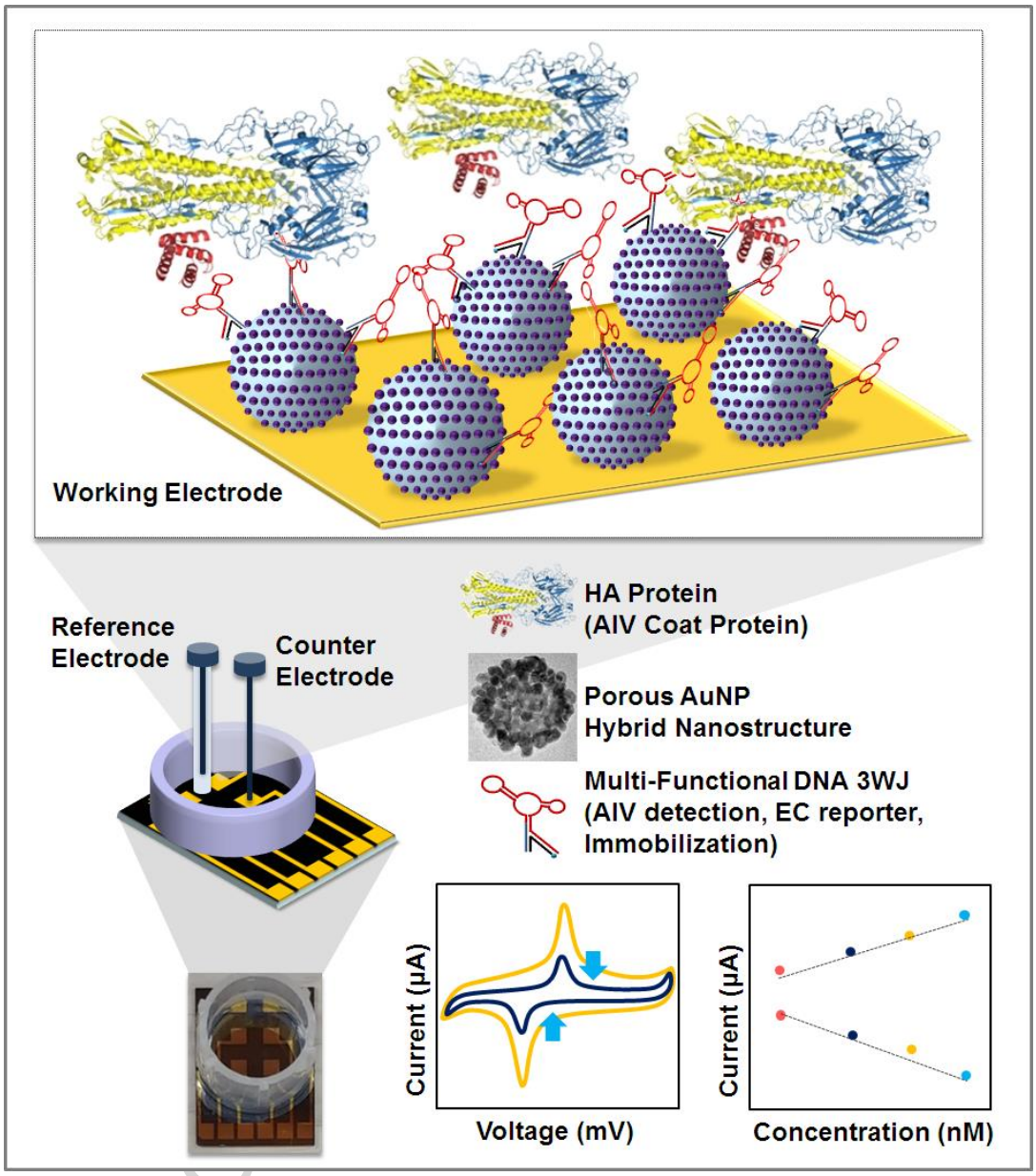

Fig. 1. Schematic image of the fabricated AIV detection biosensor

Fig. 1. Lee, et al.

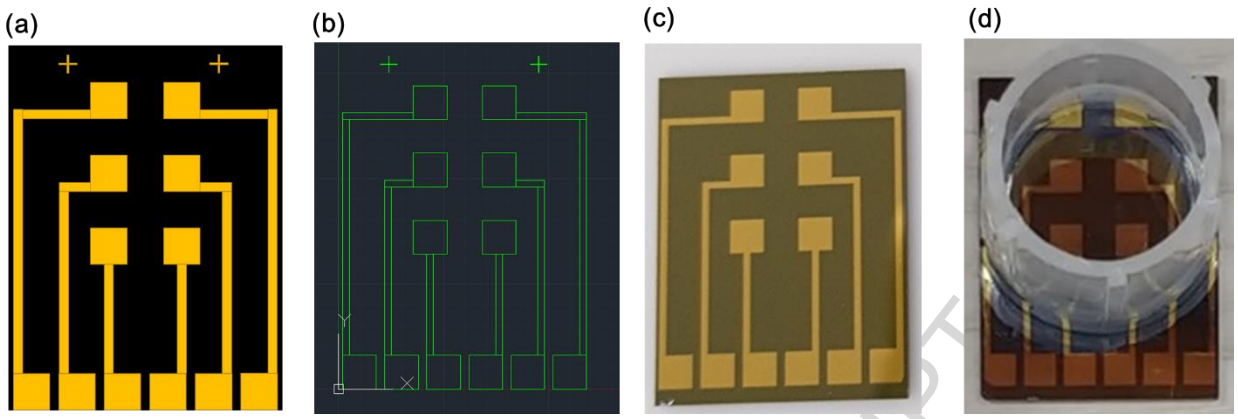

Fig. 2. (a) Schematic image of the Au electrode, (b) CAD image of Au micro-gap, (c) Real picture of Au electrode, (d) Real picture of Au electrode with working cell

Fig. 2. Lee, et al.

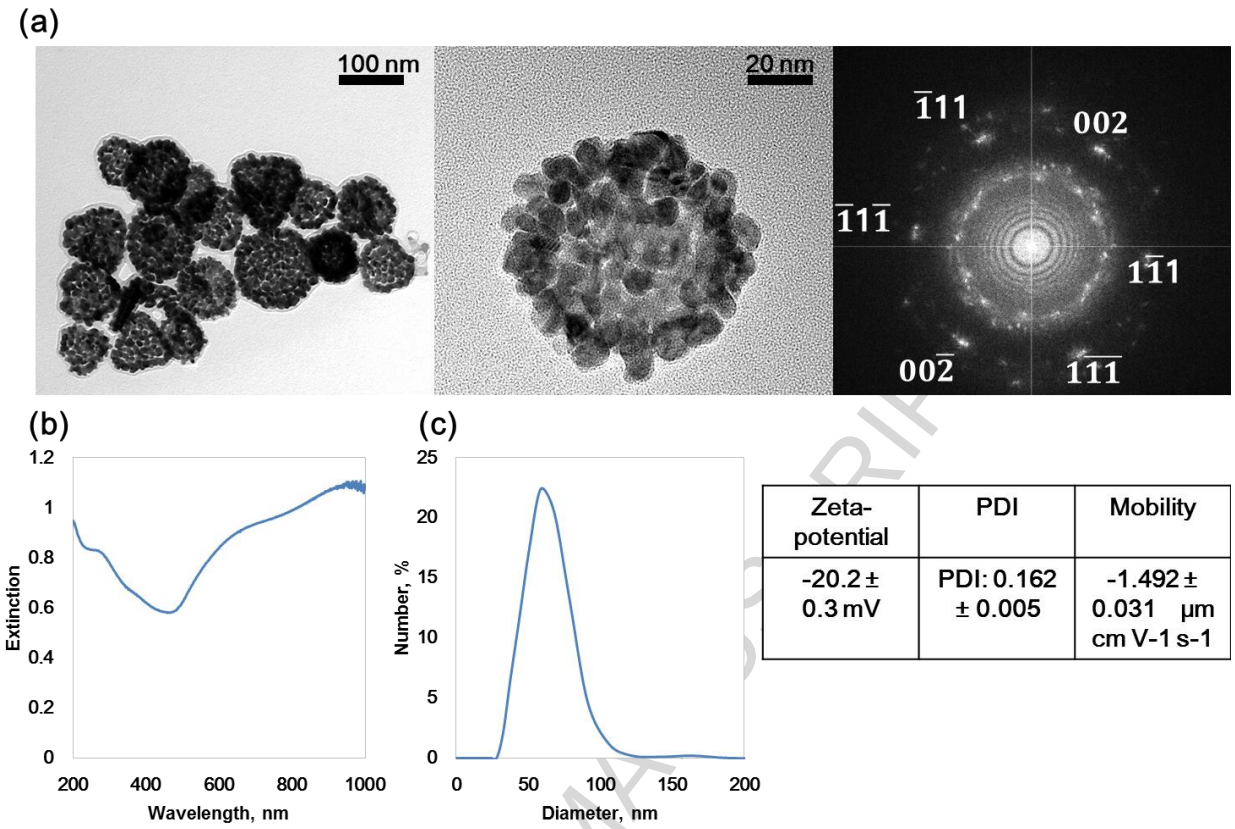

Zeta-potential	PDI	Mobility
-20.2 ± 0.3 mV	PDI: 0.162 ± 0.005	-1.492 ± 0.031 μm cm V-1 s-1

Fig. 3. (a) HR-TEM image of synthesized pAuNPs, (b) UV-VIS spectrum of synthesized pAuNP, (c) DLS result of of synthesized pAuNPs.

Fig. 3. Lee, et al.

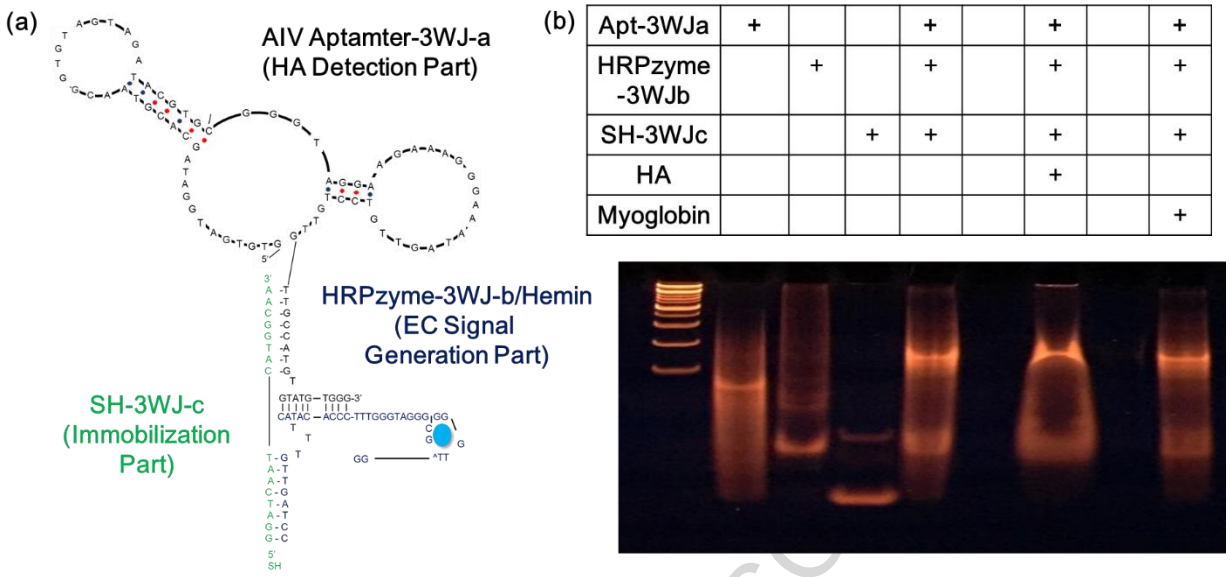

Fig. 4. (a) Schematic diagram of expected multi-functional DNA structure, (b) TBM PAGE gel result of multi-functional DNA 3WJ, HA protein, Myoglobin

Fig. 4. Lee, et al.

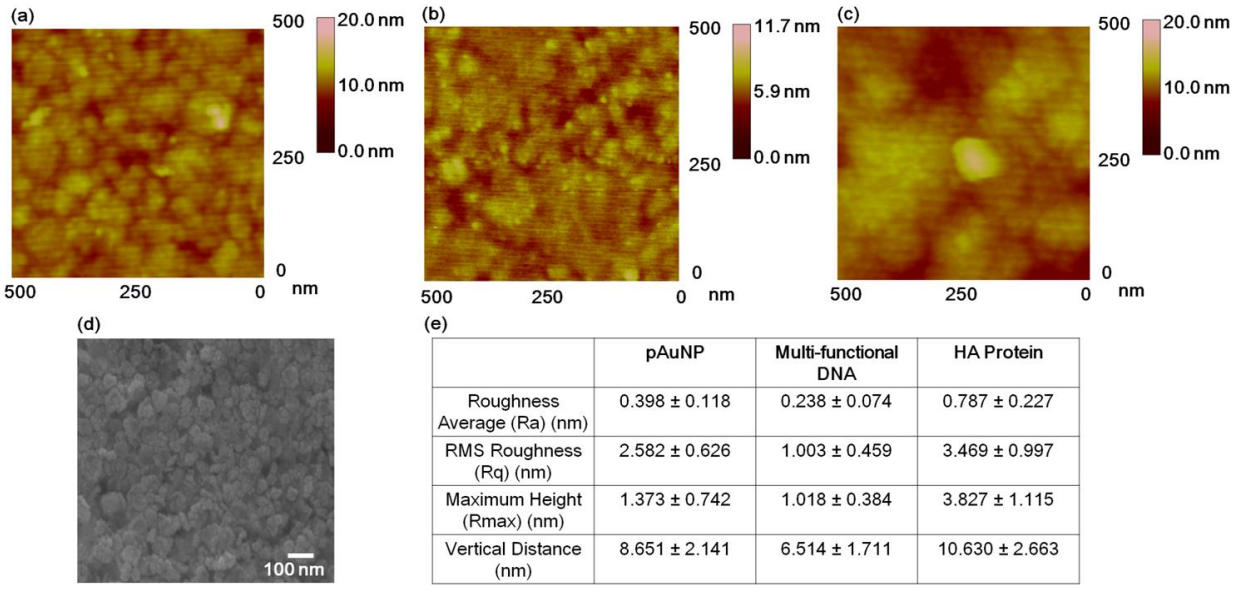

	pAuNP	Multi-functional DNA	HA Protein
Roughness Average (Ra) (nm)	0.398 ± 0.118	0.238 ± 0.074	0.787 ± 0.227
RMS Roughness (Rq) (nm)	2.582 ± 0.626	1.003 ± 0.459	3.469 ± 0.997
Maximum Height (Rmax) (nm)	1.373 ± 0.742	1.018 ± 0.384	3.827 ± 1.115
Vertical Distance (nm)	8.651 ± 2.141	6.514 ± 1.711	10.630 ± 2.663

Fig. 5. (a) Surface morphology of pAuNPs self-assembled substrate by AFM, (b) Surface morphology of DNA 3WJ on pAuNPs self-assembled substrate by AFM, (c) Surface morphology of multi-functional HA protein self-assembled substrate by AFM, (d) Surface morphology of HA protein on multi-functional DNA 3WJ/pAuNPs substrate by FE-SEM, (e) Surface roughness and vertical distance analysis of fabricated layer.

Fig. 5. Lee, et al.

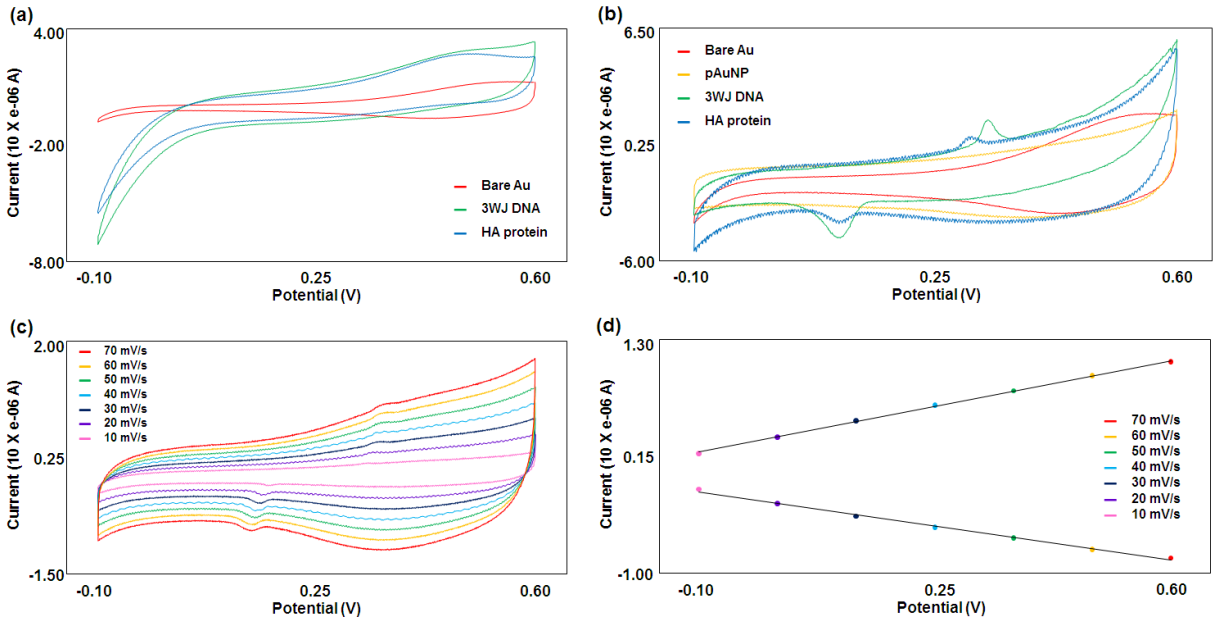

Fig. 6. (a) Cyclic voltammogram of HA protein and 3WJ-modified electrode without pAuNPs (Scan rate 50 mV/s), (b) Cyclic voltammogram of HA protein and 3WJ-modified electrode with pAuNPs (Scan rate 50 mV/s), (c) Cyclic voltammogram of 3WJ/pAuNPs immobilized on electrode in 10 mM HEPES (pH = 7.0) at different scan rate (mV/s) (d) Plots of anodic and cathodic peaks currents vs. scan rates.

Fig. 6. Lee, et al.

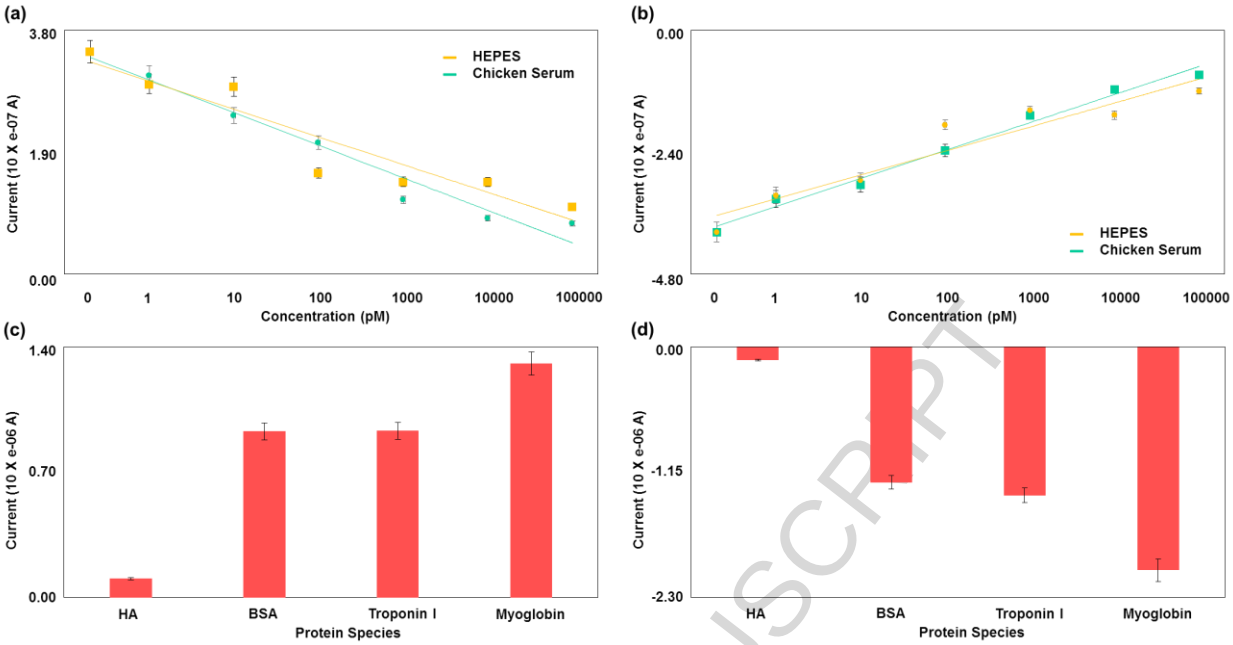

Fig. 7. (a) Oxidation peaks of the fabricated biosensor to various concentrations of target HA protein in HEPES buffer and chicken serum (0 pM to 100 nM), (b) Reduction peaks of the fabricated biosensor to various concentrations of target HA protein in HEPES buffer and chicken serum (0 pM to 100 nM), (c) Oxidation peaks of the fabricated biosensor to various target proteins in HEPES buffer (HA, BSA, Troponin I and Myoglobin), (d) Reduction peaks of the fabricated biosensor to various concentrations of target HA protein in HEPES buffer (HA, BSA, Troponin I and Myoglobin). Error bar represents relative standard deviation of 8 independent experiments.

Fig. 7. Lee, et al.

No.	Receptor Materials	Detection Method	Detection Limit	Target	Additional Signal Reporter	References
1	Aptamer	Sandwich ELAA (enzyme-linked Aptamer assay)	0.1 μg/well	HA	HRP/TMB	20
2	Aptamer	QCM	0.4 HAU	Virus	Quantum dots	10
3	Aptamer / Ag@SiO_2 nanoparticle	Fluorescence	2 ng/ml (in aqueous buffer) 3.5 ng/ml (in human serum)	HA	Thiazole orange	12
4	Aptamer	SPR	1.28 HAU	Virus	N/A	11
5	Antibody / Graphene	DPV	8.3 pM	HA	Methylene Blue	19
6	Antibody / 4,4'-thiobis benzenethiol / gold colloidal NPs	EIS, OSWV	0.6 pg/mL	Virus	$K_3[Fe(CN)_6]$	34
7	Aptamer	EIS	0.125 HAU (pure virus) 1 HAU (chicken swab samples)	Virus	Gold nanoparticle	39
8	Glycan	EIS	5 aM	Viral Particle	None	38
9	DNA 3WJ / pAuNP	CV	1 pM (in HEPES buffer) 1 pM (in chicken serum)	HA	Reporter Free	Present work

Table 1. Comparison of the fabricated biosensor with other biosensors for AI H5N1 detection in terms of receptor materials, detection method, detection limit, target and additional signal reporter.

Table 1. Lee, et al.

Graphical abstract

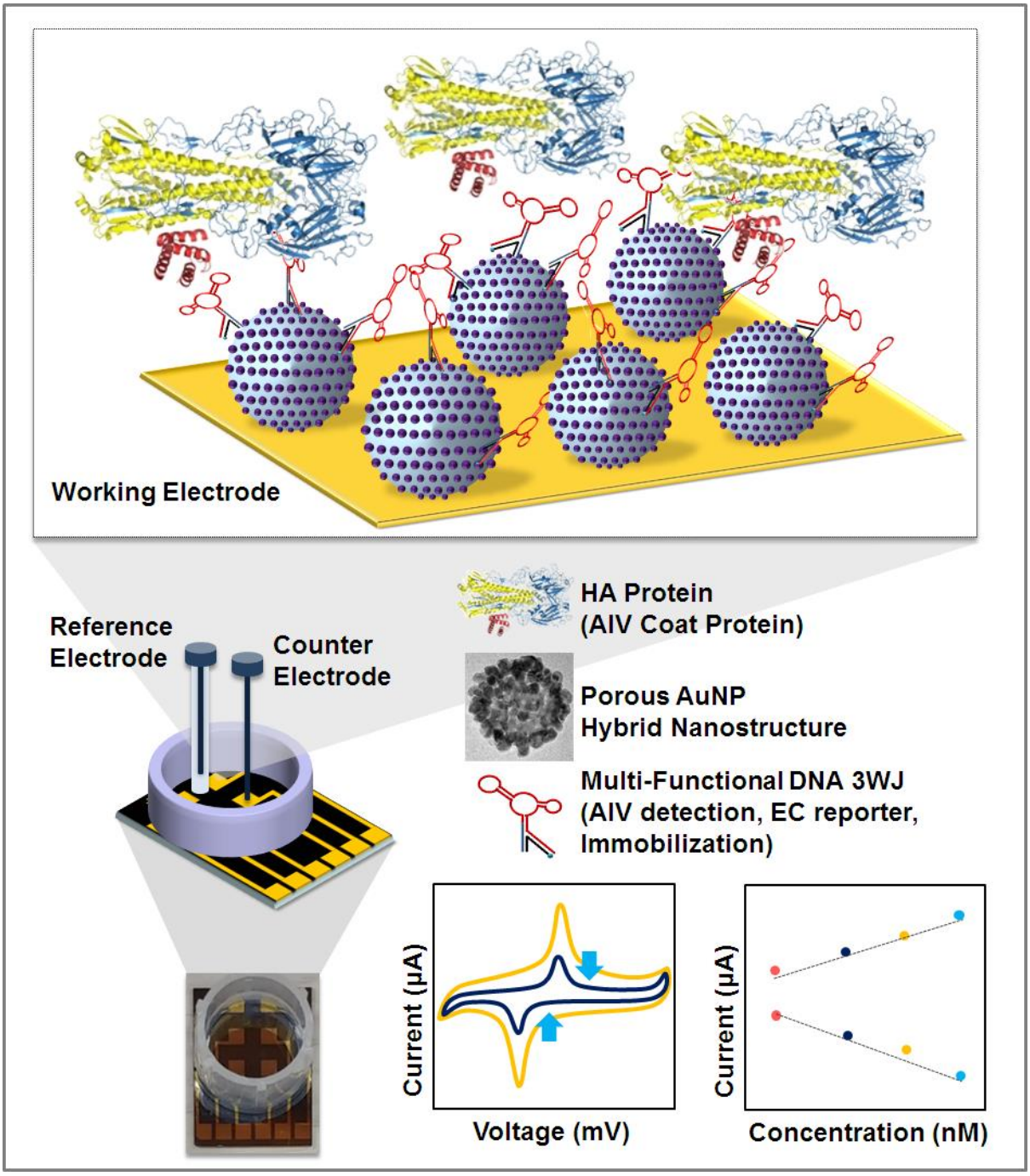

Highlights

- An electrochemical H5N1 biosensor composed of DNA 3WJ/pAuNP was developed.
- As a multi-functional bioprobe, the DNA 3WJ was introduced.
- In order to increase the electrochemical signal sensitivity, pAuNP was synthesized.
- The present study can minimize the additional amplification and labeling process.